Calculation of Weld Metal Composition Change in High-Power Conduction Mode Carbon Dioxide Laser-Welded Stainless Steels

K. MUNDRA and T. DEBROY

The use of high-power density laser beam for welding of many important alloys often leads to appreciable changes in the composition and properties of the weld metal. The main difficulties in the estimation of laser-induced vaporization rates and the resulting composition changes are the determination of the vapor condensation rates and the incorporation of the effect of the welding plasma in suppressing vaporization rates. In this article, a model is presented to predict the weld metal composition change during laser welding. The velocity and temperature fields in the weld pool are simulated through numerical solution of the Navier-Stokes equation and the equation of conservation of energy. The computed temperature fields are coupled with velocity distribution functions of the vapor molecules and the equations of conservation of mass, momentum, and the translational kinetic energy in the gas phase for the calculation of the evaporation and the condensation rates. Results of carefully controlled physical modeling experiments are utilized to include the effect of plasma on the metal vaporization rate. The predicted area of cross section and the rates of vaporization are then used to compute the resulting composition change. The calculated vaporization rates and the weld metal composition change for the welding of high-manganese 201 stainless steels are found to be in fair agreement with the corresponding experimental results.

I. INTRODUCTION

DURING laser beam welding of many important engineering alloys, pronounced vaporization of alloying elements takes place from the weld pool surface. As a consequence, the composition of the solidified weld pool often differs significantly from that of the alloy being welded. For example, significant changes in the composition of the weld metal have been reported[1–4] in the laser welding of high-manganese stainless steels and various aluminum alloys. The problem of composition change is particularly pronounced in the welding of thin sheets[4] where lasers are most commonly used. Currently, there is no comprehensive theoretical model to predict, from fundamental principles, laser-induced metal vaporization rates and the resulting weld pool composition changes.

Because of its importance, alloying element vaporization from the weld pool has been investigated both experimentally and theoretically. Apart from the examination of the weld metal composition and structure to evaluate the direct effects of vaporization, much of the previous experimental work was based on *in situ* monitoring of the alloying element vaporization by emission spectroscopy.[5,6,7] It was found that during welding of stainless steels, the most dominant species in the vapor phase were iron, manganese, nickel, and chromium. Block-Bolten and Eagar[8] used calculations based on the Langmuir equation to demonstrate that iron and manganese were the most prominent vapor species in the welding environment. Although the rates calculated from the Langmuir equation are useful for obtaining relative vaporization rates of various alloying elements,[8] the calculated vaporization rates are significantly higher than the actual vaporization rates under commonly used welding conditions. Even at low pressures, of the order of 200 μm of Hg, the vaporization rates of pure metal drops were found[9] to be about an order of magnitude lower than the values calculated from the Langmuir equation.

The main difficulties in the calculation of the alloying element vaporization rate are the estimation of the condensation rate of the vapor species on the surface of the pool[10,11] and the determination of the effect of plasma[5,12] in the suppression of the vaporization rate. When a metal is irradiated with a very high-power density laser beam, a significant amount of vapor condensation can take place, and the kinetics of vapor condensation must be taken into account in the calculation of the net vaporization rate. Anisimov and Rakhmatulina[10] and Knight[11] derived the equations for the calculation of the vapor condensation rates for pure metals by solving the equations of conservation of mass, momentum, and energy in a thin layer adjacent to the liquid-vapor interface, known as the Knudsen layer. Chan and Majumdar[13] used Knight's results to calculate laser-induced material vaporization rates from molten aluminum, titanium, and a superalloy. In the works of Anisimov and Rakhmatulina,[10] Knight,[11] and Chan and Majumdar,[13] the temperature calculations were performed in one dimension. Furthermore, in their studies, the emphasis was on the calculation of the net vaporization rate, taking into account the condensation of vapor. DebRoy *et al.*[14] synthesized the principles of weld pool transport phenomena and the vapor-phase gas dynamics for the calculation of laser-induced vaporization of pure metals. The calculated rates were found to be in fair agreement with the experimental data. Furthermore, the independent experimental results of Collur *et al.*[15] on the effects of

K. MUNDRA, Graduate Student, and T. DEBROY, Professor, are with the Department of Materials Science and Engineering, The Pennsylvania State University, University Park, PA 16802.

Manuscript submitted February 26, 1992.

flow rate and the nature of the shielding gas on the vaporization rate could be explained on the basis of the model. However, in all of the previous works, the effect of plasma[9,12] was not taken into account, and no predictions of weld pool composition changes were attempted.

The work reported in this article is aimed at predicting the laser-induced composition changes in stainless steels. The weld pool temperature distribution, calculated by the numerical solution of the Navier-Stokes equations and the equations of conservation of energy, was used together with the principles of gas dynamics and mass transfer for the calculation of the vaporization rates. The pressure gradient-driven vaporization rates of alloying elements at the pool surface were determined from the equations of conservations of mass, momentum, and translational kinetic energy in the gas phase. In addition, mass-transfer rates due to concentration gradients were determined using available correlations among various dimensionless numbers. The results of carefully controlled physical modeling experiments obtained in our laboratory[9,12] were used to incorporate the effect of plasma on the vaporization rate. The predicted composition changes were compared with the corresponding experimentally determined values.

II. EXPERIMENTAL PROCEDURES

The details of the experimental procedure and the experimental data used for the validation of the model are presented in our previous publications.[4,16] A carbon dioxide laser was used to irradiate samples of AISI 201 steel, as shown in Figure 1. The total rate of alloying element vaporization was determined from the measured values of the loss in sample weight and the laser material interaction time. The interaction time was recorded by an electronic chronometer suitably connected to a movable specimen table to obtain automatic clock start and stop features. A portion of the vaporized material was collected as condensate on the inner surface of a hollow, cylindrical, open-ended quartz tube which was held stationary and coaxial with the laser beam. The composition of the condensate was determined by atomic absorption (AA) spectroscopy. The rates of vaporization of the individual alloying elements were determined from the total vaporization rate and the composition of the condensate.

III. THEORETICAL INVESTIGATIONS

A. *Heat Transfer and Fluid Flow in the Molten Pool*

The change in the composition of a weld pool is a strong function of the rate of vaporization of the alloying elements and the volume of the molten metal. The rates of vaporization of the various alloying elements from the weld pool are largely dependent on the temperature distribution at the pool surface. Direct reliable measurements of temperature profile at the pool surface are difficult, since the weld pool is small in size and is often covered by an intense plasma[5,6,7] which interferes with most noncontact temperature measurement procedures. Procedures based on the selective vaporization of alloying elements[2] do not provide spatial resolution of the temperature at the pool surface. A recourse is to simulate temperature fields by mathematical modeling of the essential physical features of the process. The task involves numerical solution of the Navier-Stokes equation and the equation of conservation of energy. This approach has been adopted in this article. Since the appropriate equations are well documented in standard textbooks and the boundary conditions and other details of the application of these equations to welding are available in the recent welding literature,[17,18,19] these are not presented here. Special features of the computational scheme that have been taken into account in the boundary conditions include the convective and radiative heat loss from the surface of the pool and the evaporative heat loss due to vaporization of alloying elements. Zacharia *et al.*[20] have shown that vaporization can significantly influence the temperature field on the pool surface. The local heat flux from the pool surface, J_h, in $J/m^2 \cdot s$ is given by

$$J_h = h(T_l - T_g) + \varepsilon\sigma(T_l^4 - T_g^4) + \sum_{i=1}^{n} J_i \Delta H_i \quad [1]$$

where T_l is the local weld pool surface temperature, T_g is the ambient temperature, ε is the emissivity, σ is the Stefan-Boltzmann constant, J_i is the vaporization flux of i in $kg/m^2 \cdot s$, ΔH_i is the enthalpy of vaporization of the element i in J/kg, n is the number of alloying elements, and h is the heat-transfer coefficient in $J/m^2 \cdot s \cdot K$. The heat-transfer coefficient for a gas jet impinging on a surface was derived from the graphical results of Schlunder and Gniclinski[21] and is given by the following relation:

$$h = \frac{2\mathrm{Pr}^{0.42}\mathrm{Re}^{0.5}k}{d}\left(1 + \frac{\mathrm{Re}^{0.55}}{200}\right)^{0.5} \cdot \left[0.483 - 0.108\frac{r}{d} + 7.71 \times 10^{-3}\left\{\frac{r}{d}\right\}^2\right] \quad [2]$$

where d is the diameter of the nozzle in meters, r is the radial distance on the pool surface in meters, k is the thermal conductivity of shielding gas in $J/m \cdot s \cdot K$ at temperature T_{av}, which is the arithmetic average of T_l and T_g, Re is the Reynolds number at the nozzle exit, and Pr is the Prandtl number.

B. *Vaporization Due to Pressure Gradient*

In laser processing of metals and alloys, the temperatures reached on the surface of the material often exceed the boiling point.[22,23] For example, von Allmen[24] determined molten pool temperatures in excess of boiling point for laser treatment of copper. Batanov *et al.*[25] indicated that temperatures on the surface of the laser-irradiated material can be higher than the normal boiling point. Paul and DebRoy[17] and Zacharia *et al.*[26] have reported temperatures close to the boiling point for laser welding. Khan and DebRoy[2] measured the liquid pool surface temperatures close to the boiling point from the ratio of the rates of vaporization of alloying elements. Chan and Majumdar[13] have also reported temperatures

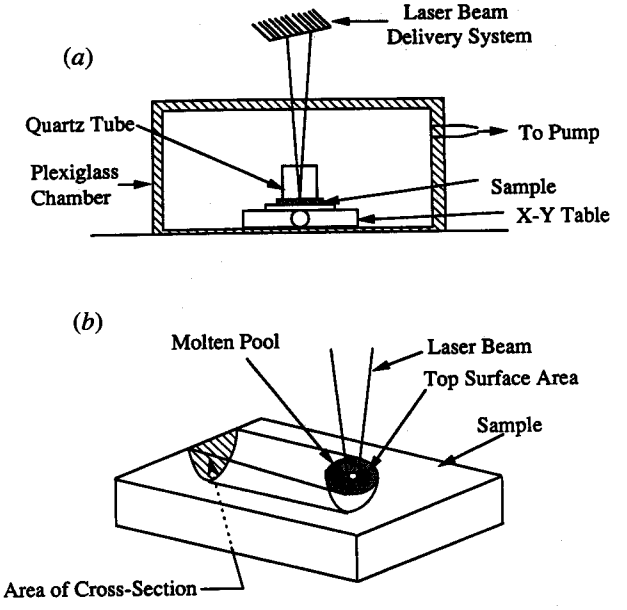

Fig. 1—Schematic diagrams of (*a*) the experimental setup and (*b*) laser material interaction.

greater than boiling point for the laser irradiation of aluminum, titanium, and a superalloy. Theoretical calculations of the vaporization rates by Knight[11] and Anisimov and Rakhmatulina[10] are based on the premise that the liquid pool surface temperatures are higher than the boiling point.

At temperatures greater than the boiling point, the pressures at the pool surface are higher than the ambient pressure, and the excess pressure provides a driving force for the vapor to move away from the surface. The velocity distribution functions of the vapor molecules, f_1, f_2, and f_3, escaping from the weld pool surface at various locations are shown schematically in Figure 2. Near the weld pool surface, the molecules cannot travel in the negative direction, and as a consequence, the distribution function is half-Maxwellian. Close to the weld pool surface, there exists a space of several mean free paths length, known as the Knudsen layer,[10,11] at the outer edge of which the velocity distribution reaches the equilibrium distribution. Here, the vapor molecule velocity, ξ, can vary from $-\infty$ to $+\infty$, as observed in Figure 2. A

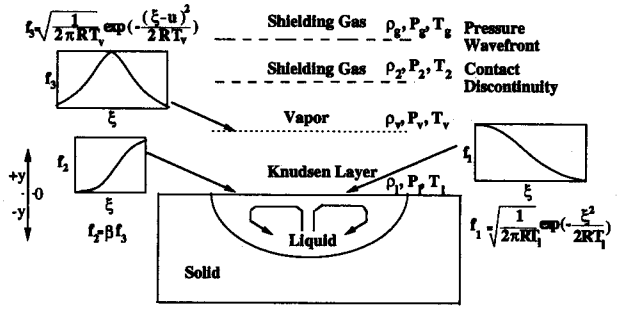

Fig. 2—A schematic diagram of the velocity distribution functions in the Knudsen layer and in adjacent regions.

portion of the vaporized material condenses on the liquid surface.

The temperature T_v, density ρ_v, pressure P_v, and mean velocity of the vapor, u, at the edge of the Knudsen layer can be related to temperature, T_l, by pressure, P_l, and the density, ρ_l, of the vapor at the liquid surface by treating the Knudsen layer as a gas-dynamic discontinuity. Anisimov and Rakhmatulina[10] and Knight[11] derived expressions for the changes in the vapor density, temperature, velocity, and the extent of condensation by using the velocity distribution functions presented in Figure 2 and solving the equations of conservation of mass, momentum, and translational kinetic energy across the Knudsen layer. Since the details of the procedure are available in their articles, only a summary of the results, commonly referred to as the jump conditions, are presented in Eqs. [3] through [5].

$$\frac{T_v}{T_l} = \left(\sqrt{1 + \pi \left(\frac{\gamma_v - 1}{\gamma_v + 1} \frac{m}{2} \right)^2} - \sqrt{\pi} \frac{\gamma_v - 1}{\gamma_v + 1} \frac{m}{2} \right)^2 \quad [3]$$

where $m = u/\sqrt{2R_vT_v}$, $R_v = R/M_v$, R is the gas constant in J/mole·K, γ_v is the ratio of specific heats of the vapor, which is treated as a monoatomic gas, and M_v is the average molecular weight of the vapor in kg/mole.

$$\frac{\rho_v}{\rho_l} = \sqrt{\frac{T_l}{T_v}} \left(\left(m^2 + \frac{1}{2} \right) e^{m^2} \operatorname{erfc}(m) - \frac{m}{\sqrt{\pi}} \right) + \frac{1}{2} \frac{T_l}{T_v} \left(1 - \sqrt{\pi}\, m e^{m^2} \operatorname{erfc}(m) \right) \quad [4]$$

where erfc is the complimentary error function.

The condensation factor, β, is given by

$$\beta = \left((2m^2 + 1) - m \sqrt{\pi \frac{T_l}{T_v}} \right) e^{m^2} \frac{\rho_l}{\rho_v} \sqrt{\frac{T_l}{T_v}} \quad [5]$$

The density, ρ_l, can be computed from P_l and T_l assuming that the vapor behaves like an ideal gas. The equilibrium vapor pressure, P_l, at the pool surface is obtained from the equilibrium vapor pressure-temperature relationships of the various alloying elements.

$$\frac{P_l}{P_g} = \sum_{i=1}^{n} a_i \frac{P_i^0}{P_g} \quad [6]$$

where P_g is the ambient pressure, a_i is the activity of the alloying element i, and P_i^0 is the equilibrium vapor pressure of the pure element i at T_l, and n is the number of alloying elements. The Knudsen layer extends only a few molecular mean free path in thickness and is filled with metal vapor. Therefore, the total pressure is determined by adding the equilibrium vapor pressures of individual components. The shielding gas is not present in this layer. Since the temperatures at the weld pool surface are very high, the activities were taken to be equal to the corresponding mole fractions. The average molecular weight of the vapor, M_v, in the Knudsen layer is given by

$$M_v = \sum_{i=1}^{n} M_i \frac{a_i P_i^0}{P_l} \quad [7]$$

where M_i is the molecular weight of species i, a_i is the activity of species i in the liquid metal, and P_i^0 is the equilibrium vapor pressure of the pure element i at T_l. Since there are four unknowns in Eqs. [3] through [5], namely, T_v, ρ_v, β, and m, it is necessary to have an additional equation to have unique values of these variables. The necessary equation is obtained by relating the pressure at the edge of the Knudsen layer to the ambient conditions. Across the Knudsen layer, the vapor wavefront moves into the shielding gas, as shown in Figure 2. The moving interface between the vapor and the shielding gas is a contact discontinuity. Across this interface, the pressures are the same; *i.e.*, $P_2 = P_v$. However, there are discontinuities in temperature and the density.[27] The pressure rise at the liquid-vapor interface propagates as a pressure wave, as shown in Figure 2. The wavefront may be treated as a pressure discontinuity, and the pressure change across the wavefront may be obtained by applying the Rankine-Hugoniot relation.[28]

$$\frac{P_l}{P_g}\frac{P_2}{P_l} = 1 + \gamma_g M\Gamma\left(\frac{\gamma_g + 1}{4} M\Gamma + \sqrt{1 + \left(\frac{\gamma_g + 1}{4} M\Gamma\right)^2}\right) \quad [8]$$

where P_g and P_2 are the pressures in front of and behind the wavefront, respectively, γ_g is the ratio of specific heats for shielding gas, and $\Gamma = \sqrt{\gamma_v R_v T_v}/\sqrt{\gamma_g R_g T_g}$. The Mach number, M, is related to m according to the equation

$$m = M\sqrt{\frac{\gamma_v}{2}} \quad [9]$$

In Eq. [8], P_l/P_g can be computed from Eq. [6] for a given local surface temperature, and since $P_2 = P_v$, for an ideal gas, P_2/P_l can be expressed as a function of m with the help of Eqs. [3] and [4]. Thus, Eq. [8] is effectively reduced to a nonlinear equation in m and can be solved iteratively or graphically to obtain m and the Mach number for a given local weld pool surface temperature. The values of T_v, ρ_v, and β, corresponding to a local temperature T_l, can be determined from Eqs. [3] through [5] by using the computed value of m. The Mach number and the density ρ_v can then be used to calculate the vaporization flux, J_p, in kg/m$^2 \cdot$ s, due to the pressure gradient at the pool surface corresponding to a local surface temperature T_l.

$$J_p = \rho_v MS \quad [10]$$

where S is the speed of sound in vapor at temperature T_v. Since the rate of vaporization of an alloying element is proportional to its partial pressure over the pool, its flux, $J_{p,i}$, is given by

$$J_{p,i} = a_i \frac{P_i^0}{P_l}\frac{M_i}{M_v} J_p \quad [11]$$

The total condensation flux, J_{cond}, in kg/m$^2 \cdot$ s, due to the excess pressure at surface temperature T_l is given by[11]

$$J_{cond} = \beta\rho_v\sqrt{\frac{R_v T_v}{2\pi}}\left(e^{-m^2} - m\sqrt{\pi}\,\text{erfc}\,(m)\right) \quad [12]$$

where β is the condensation factor defined by Eq. [5].

C. *Vaporization Due to Concentration Gradient*

At the pool surface, the concentrations of the alloying elements in the vapor are considerably higher than their respective concentrations in the bulk shielding gas. The vaporization flux of an element i due to concentration gradient, $J_{c,i}$, in kg/m$^2 \cdot$ s, is then defined as

$$J_{c,i} = K_{g,i} M_i \frac{a_i P_i^0}{\mathrm{R} T_l} \quad [13]$$

where P_i^0 is equilibrium vapor pressure of the element i over pure liquid i in atmosphere, M_i is the molecular weight of the element i in kg/kg $\cdot$ mole, R is the gas constant in m^3 atm/kg $\cdot$ mole K, and $K_{g,i}$ is the mass-transfer coefficient of the element i in m/s. The mass-transfer coefficient was derived from the graphical results of Schlunder and Gniclinski[21] and is given by

$$K_{g,i} = \frac{2\mathrm{Sc}^{0.42}\mathrm{Re}^{0.5} D}{d}\left(1 + \frac{\mathrm{Re}^{0.55}}{200}\right)^{0.5} \cdot \left[0.483 - 0.108\frac{r}{d} + 7.71 \times 10^{-3}\left\{\frac{r}{d}\right\}^2\right] \quad [14]$$

where d is the diameter of the nozzle in meters, r is the radial distance on the pool surface in meters, D is the diffusivity of the element in the shielding gas in m^2/s at temperature T_{av}, Re is the Reynolds number at the nozzle exit, and Sc is the Schmidt number of the element at average temperature T_{av}. The total vaporization flux, J_i, for an element i is then given by

$$J_i = J_{p,i} + J_{c,i} \quad [15]$$

D. *Composition Change in the Weld Pool*

If the total rate of vaporization and the rates of vaporization of the alloying elements are known, the composition of the weld metal can be predicted by simple mass balance. The final weight percent of an element i, (wt pct i)$_f$, is given by

$$(\text{wt pct } i)_f = \frac{v A \rho (\text{wt pct } i)_i - 100\int_0^r 2\pi J_i r dr}{v A \rho - \int_0^r 2\pi J r dr} \quad [16]$$

where v is the scanning speed in m/s, ρ is the density of the weld metal in kg/m^3, (wt pct i)$_i$ is the initial weight percent of an element i in the weld metal, $\int_0^r 2\pi J_i r dr$ and $\int_0^r 2\pi J r dr$ are the rates of vaporization of an element i and the total rate of vaporization, respectively, in kg/s,

and A is the area of the vertical cross section perpendicular to the scanning direction in m^2. For low laser beam scanning velocities, the weld pool top surface is approximately circular in shape. The composition change is then given by

$$(\Delta \text{ wt pct } i) = (\text{wt pct } i)_f - (\text{wt pct } i)_i \quad [17]$$

IV. RESULTS AND DISCUSSION

A. *Velocity and Temperature Fields*

Zacharia *et al.*[26] showed that in laser welding, a thermal quasi-steady state is achieved very rapidly. Mehrabian *et al.*[29] demonstrated that the time required to reach the maximum melt depth in iron for a laser power of 2×10^9 W/m^2 is of the order of 1 ms. Thus, for laser irradiation extending to several milliseconds or more, the molten pool remains in a steady state for almost the entire time span. Typical steady-state temperature and velocity fields obtained from the solution of Navier-Stokes equations and the equations of conservation of mass and energy are shown in Figure 3. The calculation takes into consideration the convective heat loss to the shielding gas and the radiative and evaporative heat losses at the pool surface. The calculations indicate that the convective and radiative heat losses are less than 1 pct of the evaporative heat loss. The average thermophysical properties and other data used for the calculations are presented in Tables I and II. The details of the calculations of thermal conductivity and viscosity of the shielding gas are presented in Appendix I. The velocity field demonstrates the importance of the convective flow on the heat transfer in the pool. For low concentrations of surface-active elements and high surface temperatures, the temperature coefficient of surface tension is negative.[30,31] Therefore, the velocities at the weld pool surface, shown in Figure 3, are radially outward, resulting in a relatively shallow pool. The maximum radial velocity is of the order of 0.9 m/s, which is close to the value reported by Zacharia *et al.*[26] and Paul and DebRoy.[17] The computed strong temperature gradient on the surface of the pool is consistent with the absorption of a significant amount of energy in a small localized area near the laser beam axis. It is observed from Figure 4 that the calculated values of the area of cross section of the weld pool for different laser powers are in good agreement with the corresponding experimental values. As indicated in Table I(b), the expansion of the laser beam radius with power was taken into account. In the range of laser powers investigated, slight adjustment of the absorption coefficient values, within ±15 pct, was necessary to obtain good agreement between the experimental and the calculated cross-sectional areas.

The peak temperatures decreased slightly with power, as can be observed from Figure 5(a), mainly because of the difference in the focusing optics and the resulting changes in beam characteristics at high laser powers. The

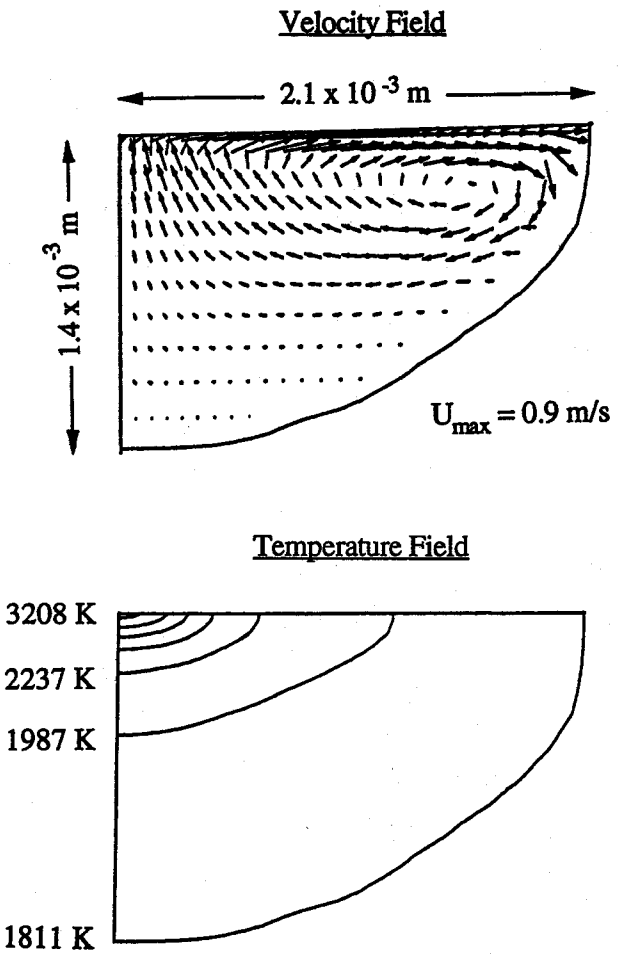

Fig. 3 — Velocity and temperature fields for a laser power of 3000 W.

Table I(a). Data Used for Calculations

Property/Parameter	Value
Density (kg/m^3)	7200
Melting point (K)	1811
Effective viscosity (kg/m · s)	3.0×10^{-2}
Thermal diffusivity of solid (m^2/s)	3.8×10^{-6}
Thermal diffusivity of liquid (m^2/s)	3.5×10^{-5}
Specific heat of solid (J/kg · K)	710.6
Specific heat of liquid (J/kg · K)	836
Temperature coefficient of surface tension (N/m · s)	-4.3×10^{-4}
Ratio of specific heats of vapor (γ_V)	1.667
Helium flow rate (m^3/s)	5.5×10^{-4}
Scanning speed of the laser (m/s)	15.24×10^{-3}
Emissivity of the pool surface	0.1

Table II. Enthalpies of Vaporization of the Alloying Elements[32]

Element	Enthalpy (kJ/kg)
Iron	6087
Manganese	4005
Chromium	6577
Nickel	6388

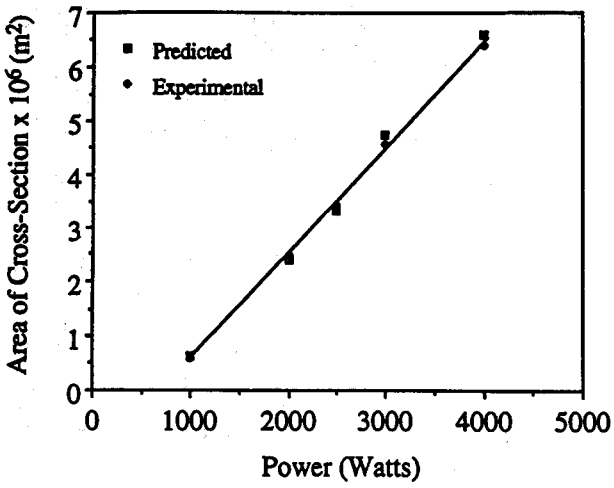

Fig. 4—Comparison of the experimental and the predicted areas of cross section.

Table I(b). Beam Radius and Absorption Coefficient Values Used for Calculations

Power (W)	Radius of the Beam (m)	Absorption Coefficient
1000	1.5×10^{-4}	0.16
2000	3.1×10^{-4}	0.19
2500	3.9×10^{-4}	0.19
3000	5.2×10^{-4}	0.20
4000	7.7×10^{-4}	0.21

computed results also demonstrate the importance of evaporative heat loss in the calculation of the peak temperature for different laser powers. It is observed from Figure 5(a) that the evaporative heat loss significantly reduces the peak temperature, and substantial errors in the calculated temperatures result if the heat loss is ignored. The computed results are consistent with the observations of Zacharia *et al.*,[20] who reported a significant drop in temperatures when evaporative heat loss from the pool surface was considered. It is observed from Figures 4 and 5(b) that both the surface area and the area of cross section of the pool increase with power. Because of the pronounced increase in the surface area, the rate of vaporization, and consequently, the heat loss due to vaporization, increases significantly with power.

B. *Vaporization Rates*

From the peak temperatures plotted in Figure 5(a), it is observed that the temperatures reached at the center of the pool are greater than the boiling point of pure iron. The temperature at which the pressure on the surface is equal to 1 atmosphere was calculated to be 2953 K from the equilibrium vapor pressure-temperature relationship for the various alloying elements presented in Appendix II and the composition of the steel indicated in Table III. When the local surface temperature is higher than this value, the pressure at the weld pool surface is greater than the ambient pressure. In such a case, the

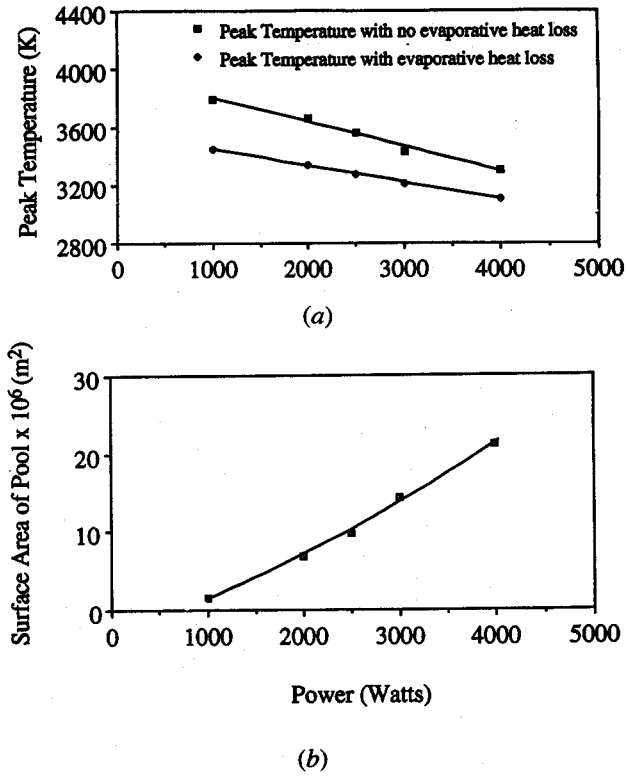

Fig. 5—(*a*) Peak temperatures with and without the evaporative heat loss *vs* power and (*b*) surface area of the pool *vs* power.

Table III. Initial and Final Compositions of the Steel after Welding*

Elements	Initial Composition (Wt Pct)	Activity (Mole Fraction)	Final Expected Composition (Wt Pct)	Expected Change (Wt Pct)
Manganese	6.50	0.066	6.16	−0.34
Chromium	17.00	0.180	16.93	−0.07
Nickel	4.25	0.041	4.28	+0.03
Iron	70.94	0.710	71.30	+0.36
Remainder	1.31	—	1.33	+0.02

*Laser power, 3000 W; welding speed, 15.24×10^{-3} m/s.

relations among the temperature, pressure, and the Mach number for a material can be represented on a plot of temperature *vs* pressure for various values of Mach number. The plot, commonly referred to as the flow state diagram, obtained from the solution of Eqs. [3] through [9], is shown in Figure 6. For a given surface temperature, the Mach number of the vapor across the Knudsen layer is uniquely defined and is given by the line that intersects the equilibrium vapor pressure curve at that temperature. For example, at 3200 K, the value of the Mach number is 0.29. The calculated variations of temperature, pressure, and density at various locations in the gas phase are presented in Figure 7. The details of the calculation procedure are given in Appendix III. The values of the Mach number and the density of the vapor across the Knudsen layer are presented in Figure 8 for various surface temperatures. The computed values of

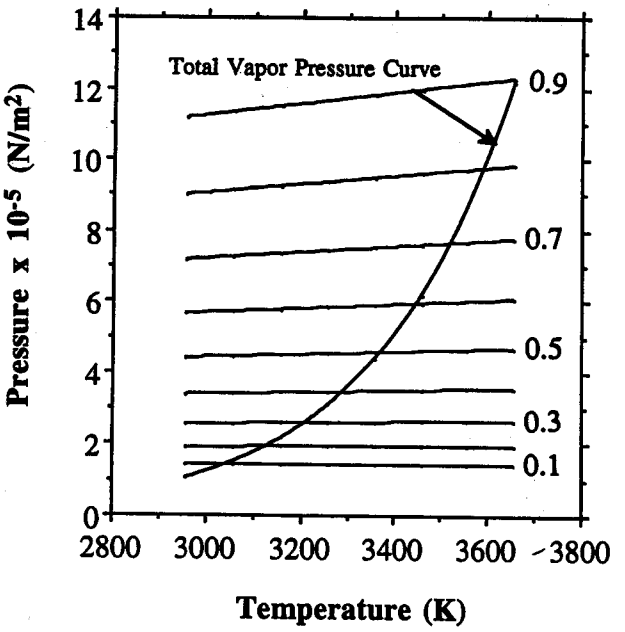

Fig. 6—Flow state diagram for AISI 201 stainless steel in helium atmosphere. The Mach numbers for various lines are indicated in the figure.

both the Mach number and the vapor density indicate their strong dependence on the surface temperature due to the direct correlation between the vapor pressure and temperature. From the values of the Mach number and the density, total vaporization flux and the flux of the individual alloying elements due to pressure gradient are calculated from Eqs. [10] and [11]. The vaporization rate due to concentration gradient is calculated from mass transport considerations. The procedure takes into account the gas flow conditions and the nature of the shielding gas in accordance with Eq. [13].

The radial distribution of the total flux and the vaporization flux of the various alloying elements due to the combined effects of total pressure and concentration gradients are plotted in Figure 9. Similarly, the radial distribution of the vaporization flux of the individual alloying elements and the total flux calculated from the Langmuir equation are plotted in Figure 10. In Figures 9 and 10, vaporization fluxes are plotted only in the region close to the center of the pool where vaporization is significant. Comparison of the results in Figures 9 and 10 indicates that the flux of the alloying elements predicted from the Langmuir equation is much higher than the corresponding value calculated in the present work.

C. *Effect of Plasma on Vaporization Rate*

During laser welding, a plasma plume is always present near the weld pool. The effect of plasma in influencing vaporization rates of metal drops was determined in our laboratory by conducting appropriate physical modeling experiments.[9,12] Figure 11(a) shows the results of these experiments. It is observed from the data that the presence of plasma lowers the vaporization rate significantly. In the plasma, both the excited neutral and

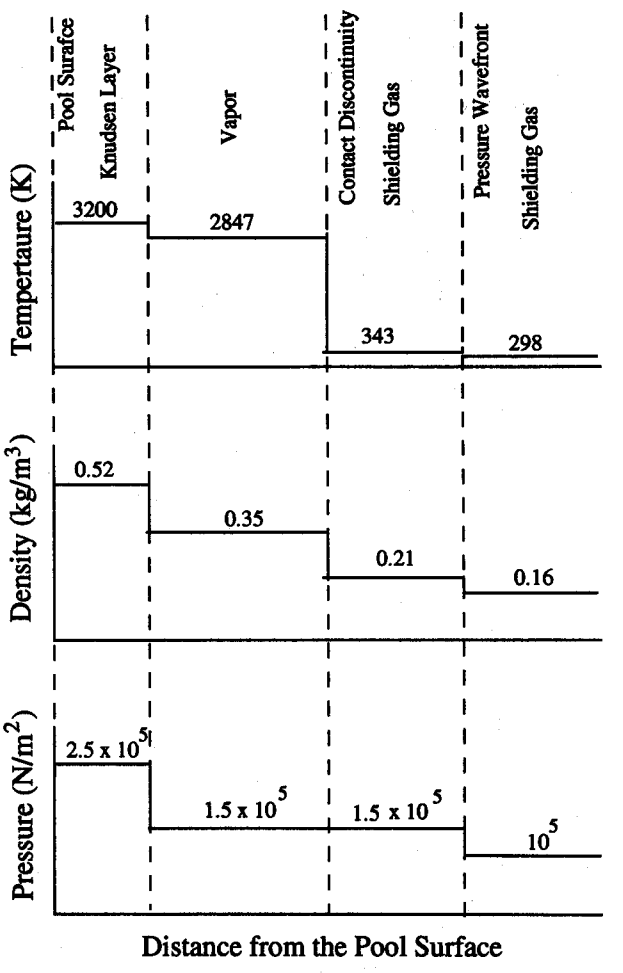

Fig. 7—Values of temperature, pressure, and density at various locations in the gas phase for a pool surface temperature of 3200 K.

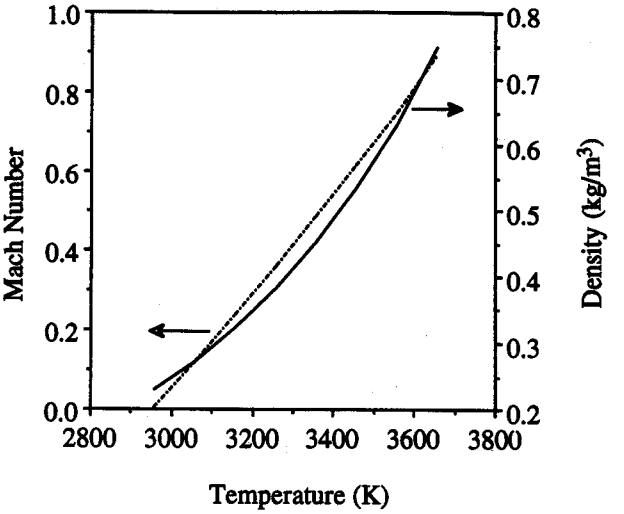

Fig. 8—Mach number and density for AISI 201 stainless steel for various temperatures at the edge of the Knudsen layer in helium atmosphere.

the ionized metal and shielding gas species are present along with free electrons. In view of the high mobility of the electrons among the various charged species in the system, the flux of the electrons to the liquid metal surface is far higher than the flux of the heavier species in the plasma. As a result, the liquid metal surface acquires negative charge, and the vapor near the surface becomes densely populated with positively charged ions, as shown in Figure 11(b). The attraction between the positively charged metal ions and the negatively charged vaporizing surface leads to enhanced condensation of metallic species. For iron, the vaporization rate in the presence of plasma varied from 50 to 90 pct of the vaporization rate when no plasma was present. The results of the controlled physical modeling experiments[9,12] were used to incorporate the effect of the plasma on the vaporization rate. An average of one third of the vaporized material was assumed to recondense on the surface of the material due to the space charge effect.

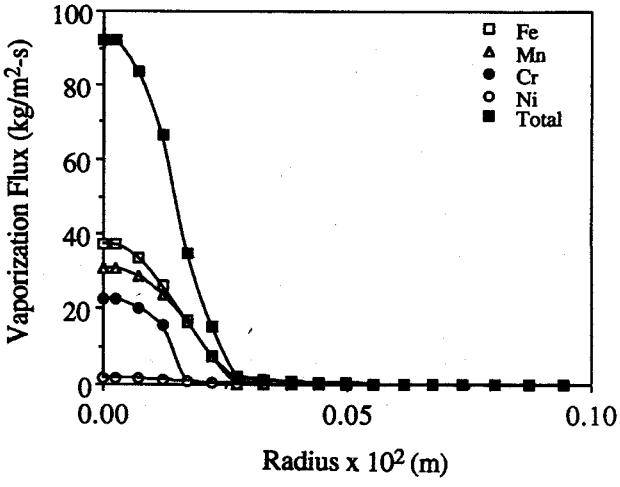

Fig. 9—Total vaporization flux and flux of various alloying elements calculated from the present model for a laser power of 3000 W.

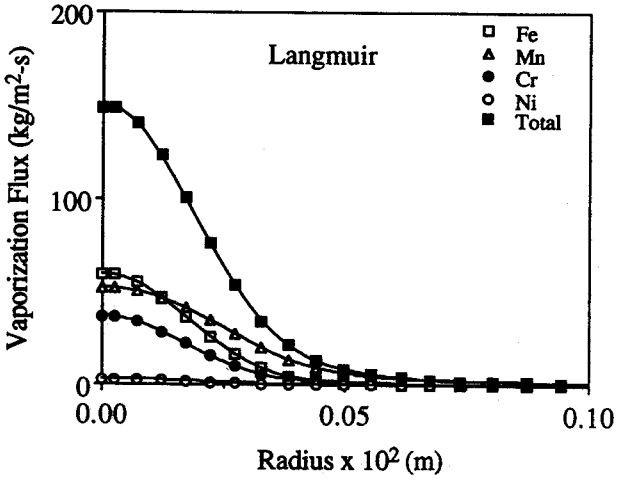

Fig. 10—Vaporization flux for various alloying elements and the total flux computed using the Langmuir equation for a laser power of 3000 W.

D. *Composition Change*

In Figure 12, the total vaporization rate computed from the model and the value calculated from the Langmuir equation are compared with the experimentally determined rate for a laser power of 3000 W. It is observed

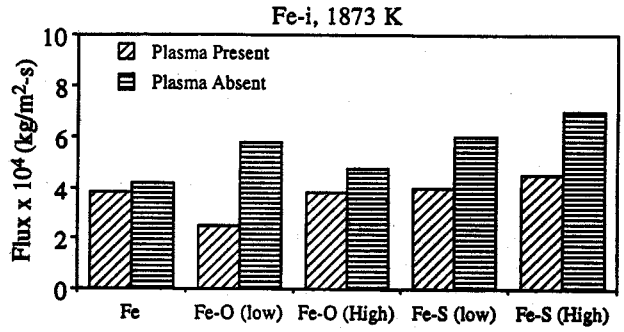

(*a*)

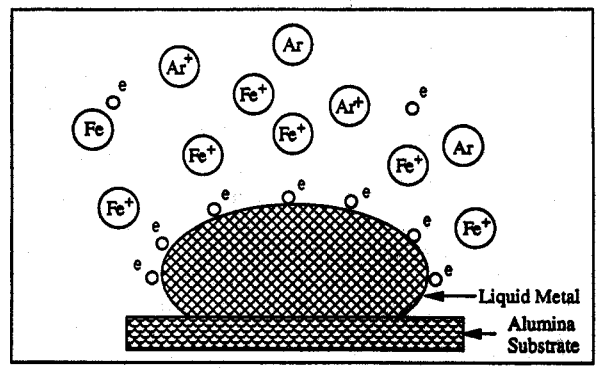

(*b*)

Fig. 11—(*a*) Vaporization flux for controlled laboratory experiments with metal drops in the presence and absence of plasma[6] and (*b*) schematic representation of the space charge effect.[6]

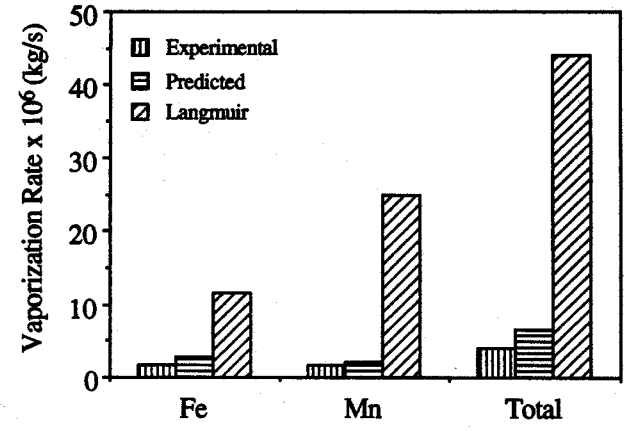

Fig. 12—Comparison of the vaporization rates calculated from the Langmuir equation and from the present model with experimentally determined values for a laser power of 3000 W.

that the computed value of the vaporization rate is in good agreement with the experimental data. The rate calculated from the Langmuir equation was significantly higher than the experimental value. Similarly, the experimentally determined rates of vaporization of Mn and Fe agreed well with the corresponding calculated results. For various laser powers, the changes in the manganese concentrations calculated from its rates of vaporization and the corresponding weld geometries are presented in Figure 13. It can be observed that the the calculated changes in manganese concentrations are in good agreement with the experimentally observed composition changes. Furthermore, the values predicted by the Langmuir equation are significantly higher than the corresponding experimental values. Although the rate of vaporization of manganese increases with power, the change in the concentration of manganese in the weld pool becomes less pronounced at high laser powers. This is because at high powers, the increase in vaporization rate is also accompanied by an increase in the volume of the weld pool. The volume increase outweighs the effect of increased vaporization rate. The expected changes in the concentrations of iron, chromium, and nickel for a laser power of 3000 W are presented in Table III. It is observed from the computed results that the concentrations of manganese and chromium decreased and those of iron and nickel slightly increased due to welding. The results are consistent with the experimental data of Khan and DebRoy[2] who found increased weight percentages of iron and nickel and decreased weight percentages of manganese and chromium in the laser-welded 202 stainless steel.

V. CONCLUSIONS

The rates of vaporization of the various alloying elements predicted by taking into account the vapor condensation and the effect of plasma were in good agreement with the experimental data. The rates predicted by the Langmuir equation were significantly higher than the actual values. An adjustment of ±15 pct of the beam absorption coefficient was necessary for different laser powers for accurate calculation of the areas of cross section of the weld pool from the principles of transport phenomena. Heat loss due to vaporization of the alloying elements significantly decreased the temperatures on the pool surface. Realistic prediction of weld pool composition change during multikilowatt conduction mode laser welding is practical if vapor condensation and the effect of plasma are taken into account in the calculations.

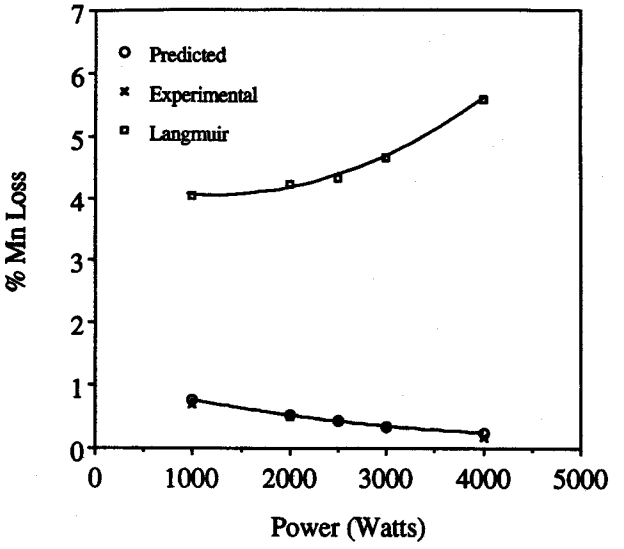

Fig. 13—Calculated and experimental changes in the manganese concentration in the weld pool.

APPENDIX I

Calculation of thermophysical properties of gas and vapor

The thermal conductivity of shielding gas is given by

$$k_g = \frac{3.9523 \times 10^{-2}}{\sigma_g^2 \Omega_k^*(T^*)} \sqrt{\frac{T}{M_g}}$$

where k_g is in J/m · s · K, σ is the collision diameter in angstroms, $T^* = k_B T/\varepsilon$, where k_B is the Boltzmann constant, ε is the intermolecular force parameter, M_g is the molecular weight of the shielding gas, and Ω_k is the slowly varying function of the dimensionless parameter kT/ε.

The viscosity of the shielding gas in kg/m · s at temperature T is given by

$$\mu_g = \frac{2.6693 \times 10^{-6}}{\sigma_g^2 \Omega_\mu^*(T^*)} \sqrt{M_g T}$$

where Ω_μ is again a slowly varying function of the dimensionless parameter kT/ε.

The mass diffusivity of an element i in the shielding gas, $D_{i,g}$, at absolute temperature T is given by

$$D_{i,g} = \frac{1.8583 \times 10^{-7} \sqrt{\left(\frac{1}{M_i} + \frac{1}{M_g}\right) T^3}}{\sigma_{i,g}^2 \Omega_{D,i}(T^*)}$$

where $D_{i,g}$ is in m^2/s, M_i is the molecular weight of the element i, $\sigma_{i,g} = (\sigma_i + \sigma_g)/2$, $\Omega_{D,i}$ is a slowly varying function of $T/\varepsilon_{i,g}$, where

$$\varepsilon_{i,g} = \sqrt{(\varepsilon)_i (\varepsilon)_g}$$

The data used for the various parameters are given in Table IV. The values of Ω's were obtained from Reference 33.

Table IV. Data Used for Calculation of Diffusion Coefficients

Parameter	σ (A)	ε/k
Iron	2.43	3545.2
Manganese	2.58	2817.9
Chromium	2.46	3738.2
Nickel	2.38	3641.5
Helium	2.58	10.2

APPENDIX II

Equilibrium vapor pressure data used for the calculations

The equilibrium vapor pressures of the various vaporizing species, namely, Mn, Cr, Ni, and Fe, over the respective pure liquids, at temperature T, expressed in atmospheres were calculated using the following equations:

$$\log P^0_{Mn} = -5.58 \times 10^{-4}T - 1.503 \times 10^4/T + 12.609/1.013 \times 10^5$$

[Reference 34]

$$\log P^0_{Ni} = -3.519 \times 10^3/T + 74.94 \log T - 18.042 \times 10^{-3}T + 15.14 \times 10^{-7}T^2 - 214.297/1.013 \times 10^5$$

[Reference 35]

$$\log P^0_{Cr} = -13.505 \times 10^3/T + 33.658 \log T - 9.29 \times 10^{-3}T + 8.381 \times 10^{-7}T^2 - 87.077/1.013 \times 10^5$$

[Reference 35]

$$\ln P^0_{Fe} = -4.3734 \times 10^4/T + 13.98$$ [Reference 36]

APPENDIX III

Calculation of temperature, pressure, and density at various Locations in the gas phase

At the Pool Surface

The pressure at the pool surface, P_l, for a given surface temperature, T_l, is calculated from Eq. [6]. The density at the pool surface, ρ_l, is computed from P_l and T_l assuming that the vapor behaves like an ideal gas.

At the Edge of Knudsen Layer

Equations [3] through [9] are used to calculate the Mach number of the vapor at the edge of the Knudsen layer. The Mach number is then used in Eqs. [3] and [4] to calculate the temperature, T_v, and density, ρ_v, at the edge of the Knudsen layer. The pressure at the edge of the Knudsen layer, P_v, is equal to the pressure across the contact discontinuity, P_2, and is calculated from Eq. [8].

Across the Contact Discontinuity

The temperature across the contact discontinuity, T_2, is related to the temperature at the edge of the Knudsen layer, T_v, and is given by[27]

$$\frac{T_2}{T_v} = \frac{M_g}{M_v}\frac{\rho_v}{\rho_g}$$

where M_g is the molecular weight of the shielding gas. The pressure across the contact discontinuity, P_2, is calculated by the Rankaine-Hugoniot relationship, given by Eq. [8], which relates the pressures in front of and behind the pressure wavefront. The density across the contact discontinuity, ρ_2, is related to the ambient density, ρ_g, by the following relation:[27]

$$\frac{\rho_2}{\rho_g} = \frac{(\gamma_g + 1)(P_2/P_g) + (\gamma_g - 1)}{(\gamma_g - 1)(P_2/P_g) + (\gamma_g + 1)}$$

In the Shielding Gas

The ambient pressure, P_g, is 1×10^5 N/m^2, and the ambient temperature, T_g, is 298 K. The ambient density, ρ_g, is calculated from P_g and T_g assuming that the shielding gas behaves like an ideal gas.

ACKNOWLEDGMENT

This work was supported by the United States Department of Energy, Office of Basic Energy Sciences, Division of Materials Science, under Grant No. DE-FGO2-84ER45158.

REFERENCES

1. D.W. Moon and E.A. Metzbower: *Weld. J. Res. Suppl.*, 1983, vol. 62, pp. 53-58.
2. P.A.A. Khan and T. DebRoy: *Metall. Trans. B*, 1984, vol. 15B, pp. 641-44.
3. M.J. Cieslak and P.W. Fuerschbach: *Metall. Trans. B*, 1988, vol. 19B, pp. 319-29.
4. P.A.A. Khan, T. DebRoy, and S.A. David: *Weld. J. Res. Suppl.*, 1988, vol. 67, pp. 1-7.
5. R. Miller and T. DebRoy: *J. Appl. Phys.*, 1990, vol. 68, pp. 2045-50.
6. M.M. Collur and T. DebRoy: *Metall. Trans. B*, 1989, vol. 20B, pp. 277-86.
7. G.J. Dunn, C.D. Allemand, and T.W. Eagar: *Metall. Trans. A*, 1986, vol. 17A, pp. 1851-63.
8. A. Block-Bolten and T.W. Eagar: *Metall. Trans. B*, 1984, vol. 15B, pp. 461-69.
9. P. Sahoo, M.M. Collur, and T. DebRoy: *Metall. Trans. B*, 1988, vol. 19B, pp. 967-72.
10. S.I. Anisimov and A. Kh. Rakhmatulina: *Soviet Physics-JETP*, 1973, vol. 37, pp. 441-44.
11. C.J. Knight: *AIAA J.*, 1979, vol. 17, pp. 519-23.
12. P. Sahoo and T. DebRoy: *Mater. Lett.*, 1988, vol. 6, pp. 406-08.
13. C.L. Chan and J. Mazumdar: *J. Appl. Phys.*, 1987, vol. 62, pp. 4579-86.
14. T. DebRoy, S. Basu, and K. Mundra: *J. Appl. Phys.*, 1991, vol. 70, pp. 1313-19.
15. M.M. Collur, A. Paul, and T. DebRoy: *Metall. Trans. B*, 1987, vol. 18B, pp. 733-40.
16. P.A.A. Khan: Ph.D. Thesis, Department of Materials Science and Engineering, The Pennsylvania State University, University Park, PA, 1987.
17. A. Paul and T. DebRoy: *Metall. Trans. A*, 1988, vol. 19B, pp. 851-58.
18. G.M. Oreper and J. Szekely: *J. Fluid Mech.*, 1984, vol. 147, pp. 53-79.
19. T. Zacharia, A.H. Eraslan, and D.K. Aidun: *Weld. J. Res. Suppl.*, 1988, vol. 67, pp. 18-27.
20. T. Zacharia, S.A. David, and J.M. Vitek: *Metall. Trans. B*, 1991, vol. 22B, pp. 233-41.
21. E.U. Schlunder and V. Gniclinski: *Chem.-Ing.-Tech.*, 1967, vol. 39, pp. 578-84.
22. S.I. Anisimov, A.M. Bonch-Bruevich, M.A. El'yashevich, Ya.A. Imas, N.A. Pavlenko, and G.S. Romanvov: *Sov. Phys.—Tech. Phys.*, 1967, vol. 11, pp. 945-52.
23. F.W. Dabby and U. Paek: *IEEE J. Quantum Electronics*, 1972, vol. QE-8, pp. 106-11.

24. M. von Allmen: *Laser-Beam Interactions with Materials*, Springer-Verlag, New York, NY, 1987, p. 161.
25. V.A. Batanov, F.V. Bunkin, A.M. Prokhorov, and V.B. Fedorov: *Soviet Physics—JETP*, 1973, vol. 36, pp. 311-22.
26. T. Zacharia, S.A. David, J.M. Vitek, and T. DebRoy: *Weld. J. Res. Suppl.*, 1989, vol. 68, pp. 499-509.
27. G. Emanuel: *Gasdynamics: Theory and Applications*, AIAA Education Series, New York, 1986.
28. W. Vincenti and C. Kruger: *Introduction to Physical Gas Dynamics*, Wiley, New York, NY, 1965.
29. R. Mehrabian, S. Kou, S.C. Hsu, and A. Munitz: *AIP Conf. Proc.*, MRS, Boston, MA, 1978.
30. P. Sahoo, T. DebRoy, and M.J. McNallan: *Metall. Trans. B*, 1988, vol. 19B, pp. 483-91.
31. M.J. McNallan and T. DebRoy: *Metall. Trans. B*, 1991, vol. 22B, pp. 557-60.
32. T. Iida and R.L. Guthrie: *The Physical Properties of Liquid Metals*, Clarendon Press, Oxford, United Kingdom, 1986, p. 8.
33. J.O. Hirschfelder, C.F. Curtiss, and R.B. Bird: *Molecular Theory of Gases and Liquids*, John Wiley & Sons, Inc., New York, NY, 1954.
34. R. Hultgren, P.D. Desai, D.T. Hawkins, M. Gleiser, K.K. Kelley, and D.D. Wagman: *Selected Values of the Thermodynamic Properties of the Elements*, ASM, Metals Park, OH, 1973, pp. 6-7.
35. R.E. Honig and D.A. Kramer: *Physicochemical Measurements in Metal Research*, Interscience Publishers, New York, NY, 1970, vol. 4, pp. 505-17.
36. E.T. Turkdogan: *Physical Chemistry of High Temperature Technology*, Academic Press, New York, NY, 1980.